This article has been accepted for publication in IEEE Wireless Communications Letters. This is the author's version which has not been fully edited and content may change prior to final publication. Citation information: DOI 10.1109/LWC.2024.3496257

RIS-Assisted Joint Differential Polarization and Phase Modulation for Non-Coherent Receivers

Emad Ibrahim, Rickard Nilsson, and Jaap van de Beek

***Abstract*—This letter introduces a reconfigurable intelligent surface (RIS)-assisted modulation scheme tailored for non-coherent receivers. Employing a RIS of dual-polarized elements, we manipulate the polarization state of the reflected signals to enable a differential polarization shift keying modulation scheme while simultaneously beamforming the reflected signal towards the receiver. Subsequently, an additional differential phase shift keying (DPSK) modulation layer is superimposed under two distinct deployments, where either the source or the RIS performs the DPSK modulation. Furthermore, the analytical performance is investigated, and a comparison with benchmark schemes is evaluated.**

***Index Terms*—Reconfigurable intelligent surface, differential polarization modulation, and differential phase modulation**

I. Introduction

One of the promising reconfigurable intelligent surface (RIS) applications is to operate as a standalone information modulator. The RIS manipulates the radio frequency (RF) signals to encode information, such as with backscattering communications. Various schemes have been explored in this context, including phase [1], spatial [2], polarization [3], and reflecting [4] modulation schemes. However, most studies consider coherent receivers, wherein the channel state information (CSI) is imperative at the receiver.

RIS-assisted differential modulation schemes for non-coherent receivers are less considered in the literature. In [5], a differential reflecting modulation is discussed wherein the information is encoded in the permutation order of the RIS reflection patterns, independently of the wireless channel. However, this scheme sacrifices the crucial beamforming of the RIS [6] to counteract the significant path loss of the two-hop RIS links [7]. In [6], RIS beam training and differential phase shift keying (DPSK) modulation at the transmitter is proposed. Although this scheme facilitates non-coherent receivers, the RIS doesn't superimpose any information along the reflected signals. Moreover, RIS-aided modulation schemes at the millimetre wave (mm-wave) frequencies have mainly focused on spatial scattering modulation, where information is encoded in the indices of active scatterers during transmission [8], [9]. However, this approach relies on coherent detection and is limited by the availability of scatterers in the propagation environment. Thus, there is a research gap in RIS-aided differential modulation schemes that simultaneously attain the crucial beamforming gain of the RIS and superimpose additional data stream from the RIS side.

The authors are with the Department of Computer Science, Electrical and Space Engineering, Luleå University of Technology, 97187 Luleå, Sweden e-mail:{emad.farouk.ibrahim, rickard.o.nilsson, jaap.vandebeek}@ltu.se

We acknowledge the European Project Hexa-X-II (grant 101095759) and the InterReg Aurora project Arctic 6G for partial funding of this work.

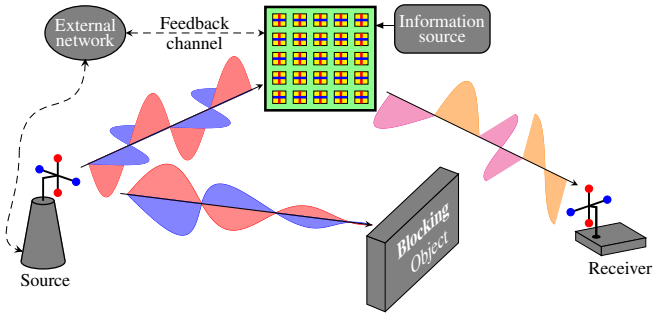

Fig. 1: Dual Polarized RIS-assisted JDPPM.

In this letter, we propose a novel RIS-assisted joint differential polarization and phase modulation (JDPPM) scheme designed for non-coherent receivers at the mm-wave frequencies. In this scheme, a RIS consisting of dual-polarized (DP) elements [10] is configured to achieve beamforming gain and shape the state of polarization (SoP) of the reflected signals, enabling a differential polarization shift keying (DPolSK) modulation. Subsequently, an additional DPSK modulation layer is superimposed. Two distinct deployments are considered. In the first scenario a feedback channel between the source and the RIS exist. The source serves as an information transmitter by performing DPSK modulation. In the second deployment, no feedback channel exists and the RIS performs the DPSK modulation, while the source operates as an RF source, akin to backscattering communications.

The main contributions of this letter are as follows. First, we demonstrate joint beamforming and SoP control of the RIS-scattered waves. Next, we exploit RIS SoP control to introduce a novel DPolSK modulation scheme. Then, we superimpose an additional DPSK modulation layer to enable a novel RIS-assisted information transfer tailored for non-coherent receivers. Subsequently, we conduct an analytical performance analysis. Finally, we validate the proposed scheme's performance and compare it with benchmark schemes.

Notations: Regular, bold lowercase and bold uppercase letters for scalars, vectors and matrices, respectively. The transpose and conjugate transpose are denoted by $(\cdot)^{\mathrm{T}}$ and $(\cdot)^{\mathrm{H}}$, respectively. $\Re\{\cdot\}$, $\Im\{\cdot\}$, $\{\cdot\}^*$, and $\{\cdot\}_{2\pi}$ denote the real part, imaginary part, complex conjugate, and the modulo 2π operation, respectively. $[\mathbf{x}]_n$ and $[\mathbf{x}]_{a:b}$ extract the nth element and the sub vector from the ath till bth elements of vector $\mathbf{x}$, respectively. $\mathrm{diag}\{\mathbf{x}\}$ and $|\mathbf{x}|_q$ denote a diagonal matrix and the l_q-norm of vector $\mathbf{x}$.

II. System Model

We consider an RIS of M DP elements, each of which consists of vertical and horizontal polarization sub-elements [10]. The RIS serves as a modulator source by encoding the reflected signals. The source and the receiver have a DP antenna consisting of vertical and horizontal polarized elements, as shown in Fig. 1. The direct channel between the source and the receiver is assumed to be blocked, which can frequently occur at the considered mm-wave frequencies.

A. Channel Model

The composite channel between the source and the receiver via the scattering on the RIS elements is defined as

$$\mathbf{H} = \sum_{m=1}^{M} \mathbf{H}_{2,m} \Phi_m \mathbf{H}_{1,m}, \tag{1}$$

where Φ_m denotes the reflection matrix of the mth element, defined as $\Phi_m = \text{diag}[e^{j\varphi_{m,\text{V}}}, e^{j\varphi_{m,\text{H}}}]$, with $\varphi_{m,\text{V}}$ and $\varphi_{m,\text{H}} \in [0, 2\pi]$, $\forall\, m \in \mathcal{M} = \{1, 2, ..., M\}$ represent the phase shifts induced by the mth element for the vertical and horizontal sub-elements, respectively. Additionally, $\mathbf{H}_{1,m} \in \mathbb{C}^{2\times 2}$ and $\mathbf{H}_{2,m} \in \mathbb{C}^{2\times 2}$ are the channels between the mth DP element to the source and the receiver, respectively.

In this letter, we consider a LoS environment given the mm-wave frequencies, wherein the orthogonality between an orthogonal SoP pair is preserved while propagating in the wireless channel [11]. However, because of the distinct orientations of the DP signals and destination, a SoP rotation often takes place. Therefore, for the second link from the RIS to the receiver, we introduce a rotation matrix to characterize the relative orientation between the RIS and receiver as

$$\mathbf{R} = \begin{bmatrix} \cos(\beta) & \sin(\beta) \\ -\sin(\beta) & \cos(\beta) \end{bmatrix}, \tag{2}$$

where β denotes the SoP rotation angle. Then, we introduce the propagation phase shift and path loss of the RIS to receiver channel [12] as $\mathbf{H}_{2,m} = \rho_2 e^{-j\mu_{2,m}} \mathbf{R}$, where ρ_2 represents the channel gain and $\mu_{2,m}$ denotes the propagation phase shift with respect to the mth element which can be modelled using the plane wave propagation model [13] as $\mu_{2,m} = \mathbf{g}_m^{\text{T}} \mathbf{q}_2$, with $\mathbf{g}_m \in \mathbb{R}^{3\times 1}$ is the Cartesian coordinates of the mth element in the RIS and $\mathbf{q}_2$ is the wave vector accounts for the phase variations over the RIS for the reflected wave as

$$\mathbf{q}_2 = \frac{2\pi}{\lambda_c} \left[\sin\zeta_2 \cos\vartheta_2, \sin\zeta_2 \sin\vartheta_2, \cos\zeta_2\right]^{\text{T}}, \tag{3}$$

with λ_c denotes the carrier wavelength, $\zeta_2 \in [0, \pi]$ and $\vartheta_2 \in [0, 2\pi]$ represent the elevation and azimuth angles of departure (AoD) from the RIS to receiver. Additionally, we assume that the source-to-RIS channel is perfectly aligned in terms of the SoP rotation, which can be achieved by adjusting the orientation of the static source and RIS before operation. As a consequence, the source-to-RIS can be represented as $\mathbf{H}_{1,m} = \rho_1 e^{-j\mu_{1,m}} \mathbf{I}_2$, $\forall\, m \in \mathcal{M}$, where ρ_1 denotes the channel gain and $\mu_{1,m}$ represents the propagation phase shift which is defined similar to the second link as $\mu_{1,m} = \mathbf{g}_m^{\text{T}} \mathbf{q}_1$, with $\mathbf{q}_1$ is the wave vector of the first channel, similar to (3) but in terms of the elevation and azimuth angles of arrivals (AoA) from the source to RIS denoted as ζ_1 and ϑ_1, respectively. Thus, given the first hop and second hop channels, the received signal at the ith transmission slot becomes

$$\mathbf{y}_i = \mathbf{H}\mathbf{x}_i + \mathbf{w}_i = \rho \sum_{m=1}^{M} e^{-j\mu_m} \mathbf{R} \Phi_m^{(i)} \mathbf{x}_i + \mathbf{w}_i, \tag{4}$$

where $\mathbf{x}_i \in \mathbb{C}^{2\times 1}$ denotes the transmitted signal, $\mathbf{w}_i \in \mathbb{C}^{2\times 1} \sim \mathcal{NC}(0, N_o \mathbf{I}_2)$ is the additive white Gaussian noise of variance N_o, $\mu_m = \mu_{1,m} + \mu_{2,m}$ is the overall phase shift through the mth element, and $\rho = \rho_1 \rho_2$ is the overall channel gain which is modeled given the plate-scattering propagation model and the radiation pattern of reflecting elements presented in [7], as

$$\rho = \left(\frac{\Delta_r \sqrt{G_t G_r}}{4\pi d_1 d_2}\right) \left[\cos(\psi_1)\cos(\psi_2)\right]^{0.285}, \tag{5}$$

where G_t and G_r denote the gains of the source and receive antennas, respectively, while $\Delta_r = \lambda_c^2/4$ is the physical area of the square-shaped reflecting element with a half-wavelength side length. In addition, d_1 and d_2 are the distances from the RIS to the source and receiver, respectively. Furthermore, ψ_1 and ψ_2 are the angles between the normal direction of the RIS to the incident and reflected waves, respectively.

B. Signal Model

We consider a transmitted signal from the source $\mathbf{x}_i = \sqrt{P_t/2}\mathbf{1}_2 s_i$, where $\mathbf{1}_2 = [1, 1]^{\text{T}}$, such as the source DP antenna shares a single RF chain, and $s_i \in \mathbb{C}$ is the modulated symbol with $\mathbb{E}\left[\mathbf{x}_i^{\text{H}} \mathbf{x}_i\right] = P_t$ denotes the transmitted power. Accordingly, the received signal in (4) simplifies to

$$\mathbf{y}_i = \mathbf{R}\mathbf{u}_i + \mathbf{w}_i, \tag{6}$$

where $\mathbf{u}_i$ is the resultant scattered wave from the RIS as

$$\mathbf{u}_i = \sqrt{\frac{\rho^2 P_t}{2}} s_i \sum_{m=1}^{M} e^{j\left(\varphi_{m,\text{H}}^{(i)} - \mu_m\right)} \begin{bmatrix} e^{j\Delta\varphi_m^{(i)}} \\ 1 \end{bmatrix}, \tag{7}$$

where $\Delta\varphi_m^{(i)} = \varphi_{m,\text{V}}^{(i)} - \varphi_{m,\text{H}}^{(i)}$ is the phase difference between the vertical and horizontal phase shifts of the mth element. To attain the crucial RIS beamforming, the operation is commonly divided into two phases: the beam training phase and the modulation phase. During the beam training phase [14], the RIS sweeps over a pre-defined codebook. Then, the optimum beam which maximizes the received signal strength is selected and fed to the RIS through an external network, as illustrated in Fig. 1. Our main interest lies in the modulation phase, while the beam training procedure is beyond the scope of this letter. Thus, to show the upper bound performance, we assume that the AoA and AoD of the first and second hop links are known. Accordingly, the RIS is first configured to coherently combine all the scattered waves with

$$\varphi_{m,\text{H}}^{(i)} = \mu_m + \omega_i \quad \text{and} \quad \varphi_{m,\text{V}}^{(i)} = \varphi_{m,\text{H}}^{(i)} + \delta_i \quad \forall\, m \in \mathcal{M}, \tag{8}$$

where ω_i and δ_i are two constant phases to be configured in the next section for enabling the JDPPM scheme. Consequently, the resultant scattered wave from the RIS becomes

$$\mathbf{u}_i = \sqrt{\frac{\rho^2 M^2 P_t}{2}} e^{j\omega_i} s_i \begin{bmatrix} e^{j\delta_i} \\ 1 \end{bmatrix}. \tag{9}$$

III. Joint Differential Polarization and Phase Modulation

In this section, we provide a fundamental background on the SoP of electromagnetic (EM) waves using the Stokes vector and Poincaré space. Then, we describe the proposed JDPPM modulation scheme.

A. Polarization of EM waves

The SoP of an EM wave can be described using the Stokes vector which is defined for a DP signal $\mathbf{e} = [e_{\mathrm{V}}, e_{\mathrm{H}}]^{\mathrm{T}}$ as [15]

$$\mathbf{s}_{\mathbf{e}} = \begin{bmatrix} s_{\mathbf{e}_0} \\ s_{\mathbf{e}_1} \\ s_{\mathbf{e}_2} \\ s_{\mathbf{e}_3} \end{bmatrix} = \begin{bmatrix} |e_{\mathrm{H}}|^2 + |e_{\mathrm{V}}|^2 \\ |e_{\mathrm{H}}|^2 - |e_{\mathrm{V}}|^2 \\ 2\Re\{e_{\mathrm{H}} e_{\mathrm{V}}^*\} \\ -2\Im\{e_{\mathrm{H}} e_{\mathrm{V}}^*\} \end{bmatrix}, \tag{10}$$

where $s_{\mathbf{e}_0}$ represents the power of the signal and $\bar{\mathbf{s}}_{\mathbf{e}} = [s_{\mathbf{e}_1}, s_{\mathbf{e}_2}, s_{\mathbf{e}_3}]^{\mathrm{T}}$ is the Stokes sub-vector which fully describes the SoP of the signal and facilitates its Cartesian mapping into the 3D Poincaré sphere. The Poincaré sphere serves as a vital tool for visually interpreting the SoP as it represents a constellation diagram for polarization modulation. In Fig. 2, the Poincaré sphere is shown where every possible SoP can be represented by a single point in the Poincaré space. Two SoPs are orthogonal to each other if the line connecting them passes through the origin [16].

B. Differential Polarization Shift Keying Modulation

The Stokes sub-vector of the scattered wave in (9) becomes $\bar{\mathbf{s}}_{\mathbf{u}_i} = [0, \gamma\cos(\delta_i), \gamma\sin(\delta_i)]^{\mathrm{T}}$, where $\gamma = \rho^2 M^2 P_t$ is the total received power and δ_i is the tuning parameter for the SoP of the scattered wave. In particular, $\delta_i \in [0, 2\pi]$ configures the SoP along the blue circle in the $s_2 - s_3$ plane shown in Fig. 2. Therefore, an orthogonal SoP pair can be configured given a π difference in δ_i. In DPolSK modulation, the variation in SoPs between two consecutive received signals is utilized to encode information. Thus, non-coherent detection becomes feasible, provided that the wireless channel remains static across two successive receiving slots. Accordingly, δ_i is configured to alternate the SoP of the scattered wave between two orthogonal SoPs as

$$\delta_i = \begin{cases} \{\delta_{i-1} + \pi\}_{2\pi} & \text{if } b_i = 1 \\ \delta_{i-1} & \text{if } b_i = 0 \end{cases}, \tag{11}$$

where b_i is the data bit of the ith time-slot. The RIS alternates the SoP between an orthogonal SoP pair. Specifically, it either maintains or changes the SoP of the current scattered wave relative to the previous one when $b_i = 0$ and $b_i = 1$, respectively. The initial SoP can be chosen freely as $\delta_0 \in [0, 2\pi]$.

C. Differential Phase Shift Keying Modulation

We superimpose an additional DPSK modulation layer over the existing DPolSK modulation. The received signal in (6) can be reformulated using (9) as

$$\mathbf{y}_i = \tilde{s}_i \mathbf{R}\bar{\mathbf{u}}_i + \mathbf{w}_i = \tilde{s}_i \mathbf{z}_i + \mathbf{w}_i, \tag{12}$$

where $\tilde{s}_i = e^{j\omega_i} s_i$ and $\bar{\mathbf{u}}_i = \sqrt{\gamma/2}[e^{j\delta_i}, 1]^{\mathrm{T}}$. As noted from $\bar{\mathbf{s}}_{\mathbf{u}_i}$, the SoP of the scattered wave is independent of $\tilde{s}_i$.

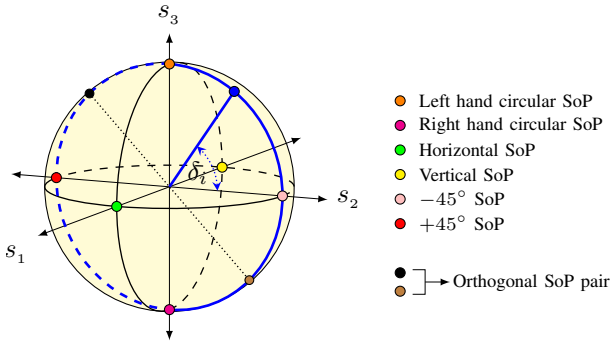

Fig. 2: Poincaré sphere.

Therefore, $\tilde{s}_i$ can be utilized to enable an additional DPSK modulation layer. Any differential modulation scheme requires a static channel over at least two consecutive time slots. However, $\mathbf{z}_i = \mathbf{R}\bar{\mathbf{u}}_i$ varies across time slots to implement the DPolSK scheme. Nevertheless, the RIS generates only two SoPs as δ_i in (11) varies between two possible values given the binary DPolSK, such as $\delta_i \in \{\bar{\delta}_1, \bar{\delta}_2\}$. Consequently, $\bar{\mathbf{u}}_i$ alternates between two possible vectors. This enables a solution by developing two parallel DPSK modulation layers separately over the two utilized SoPs. Accordingly, we define a vector $\mathbf{v} \in \mathbb{Z}^{T\times 1}$ to indicate the time slots of the first and second SoPs along a transmission frame of length T, such that $[\mathbf{v}]_i = 1$ when $\delta_i = \bar{\delta}_1$ and $[\mathbf{v}]_i = 0$ when $\delta_i = \bar{\delta}_2$. In this case, $\mathbf{z}_i$ is fixed with respect to each of the individual DPSK layers as long as the orientation of the receiver ($\mathbf{R}$) remains constant during two consecutive slots that utilize the same SoP.

However, the availability of $\mathbf{v}$ at the source is contingent upon the existence of a feedback channel between the source and RIS. Therefore, two distinct deployments are presented based on the feedback channel availability. First, when the channel exists, the source serves as the information transmitter by encoding s_i to perform the DPSK modulation, while the RIS neutralizes its impact on the phase of $\tilde{s}_i$ by setting ω_i constant. In the second deployment, when there is no feedback channel, the source transmits an unmodulated signal, $s_i = 1$, while the RIS exploits $e^{j\omega_i}$ to perform the DPSK modulation.

In both deployments, the objective is to modulate $\tilde{s}_i$ which can be accomplished as follows. First, the information bits undergo $K-$PSK modulation scheme. Then, the symbols are divided into two streams, each corresponding to a distinct SoP. Let $\bar{\mathbf{s}}_1 = [\bar{s}_{1,1}, \cdots, \bar{s}_{1,T_1-1}]^{\mathrm{T}}$ and $\bar{\mathbf{s}}_2 = [\bar{s}_{2,1}, \cdots, \bar{s}_{2,T_2-1}]^{\mathrm{T}}$ denote the PSK streams over the first and second SoP, respectively, where $T_1 = |\mathbf{v}|_0$ and $T_2 = T - T_1$. Subsequently, each stream is differentially encoded separately as

$$s'_{l,t} = \begin{cases} \bar{s}_o & \text{if } t = 1 \\ \bar{s}_{l,t-1} s'_{l,t-1} & \text{if } t > 1 \end{cases}, \tag{13}$$

where $l \in \{1, 2\}$ and $\bar{s}_o \in \mathbb{C}$ is an initial symbol for the DPSK modulation. Finally, the two independent differential modulated streams are allocated along their corresponding SoP time slots as

$$\tilde{s}_i = \begin{cases} s'_{1,t'_{1,i}} & \text{if } [\mathbf{v}]_i = 1 \\ s'_{2,t'_{2,i}} & \text{if } [\mathbf{v}]_i = 0 \end{cases}, \tag{14}$$

where $t'_{1,i} = |[\mathbf{v}]_{1:i}|_0$ and $t'_{2,i} = i - |[\mathbf{v}]_{1:i}|_0$.

IV. Non-Coherent Detection

We address non-coherent receiver that lacks partial or full CSI. Hence, we propose a two-stage detector wherein the DPolSK detection is initially executed, followed by the DPSK detection. The DPolSK detector leverages the Stokes space to detect the change in the SoP between two successive received signals. Any orthogonal SoP pair forms a line passing through the origin in the Stokes space [16]. Moreover, the orthogonality among the SoP pairs generated by the RIS is preserved in the LoS channel [11]. Therefore, the DPolSK detection can be accomplished using the Stoke sub-vectors of two successive received signals as [16]

$$\hat{b}_i = \begin{cases} 0 & \text{if } \bar{\mathbf{s}}_{\mathbf{y}_i}^{\mathrm{T}} \bar{\mathbf{s}}_{\mathbf{y}_{i-1}} \geq 0 \\ 1 & \text{if } \bar{\mathbf{s}}_{\mathbf{y}_i}^{\mathrm{T}} \bar{\mathbf{s}}_{\mathbf{y}_{i-1}} < 0 \end{cases}, \tag{15}$$

where $\bar{\mathbf{s}}_{\mathbf{y}_i}$ denotes the Stoke sub-vectors of the received signal $\mathbf{y}_i$. The detection of DPSK can be acquired based on the detected DPolSK. Initially, using the detected DPolSK bits, the time slots of each of the two orthogonal SoPs are detected to infer estimation for $\hat{\mathbf{v}}$. Next, the received signal is split over their corresponding SoP's time slots, similar to the modulation procedure, resulting in $\mathbf{Y}_l = [\mathbf{y}_{l,1}, \cdots, \mathbf{y}_{l,\hat{T}_l}]$, where $l = 1$ and $l = 2$ for the first and second SoPs, respectively. Then, for each SoP, equalization and maximum likelihood detection are performed over two successive received signals as

$$\arg \min_{\hat{s}_{l,t} \in \{s_1, \ldots, s_K\}} \left| \mathbf{y}_{l,t-1}^{\mathrm{H}} \mathbf{y}_{l,t} - (\mathbf{y}_{l,t-1}^{\mathrm{H}} \mathbf{y}_{l,t-1}) s_{l,t} \right|^2. \tag{16}$$

Also, the detection complexity is evaluated by analyzing the real multiplications and additions required in the two-stage detector. First, the DPolSK detector computes the Stokes sub-vector and then performs detection based on (15), requiring $13T$ multiplications and $7T$ additions. Next, the DPSK detector in (16) involves $(16{+}6K)T$ multiplications and$(12{+}5K)T$ additions. Thus, the overall computational complexity amounts to $(29 + 6K)T$ multiplications and $(19 + 5K)T$ additions.

V. Analytical Performance

The performance of the DPSK modulation depends on the DPolSK detector in terms of estimating the time instants for each of the SoP pairs, $\hat{\mathbf{v}}$. Thus, the bit error probability of the DPSK can be approximated as

$$P_{\text{DPSK}} \approx 0.5 P_{\text{DPoLSK}} + (1 - P_{\text{DPoLSK}}) P_{\text{DPSK|DPoLSK}}, \tag{17}$$

where P_{DPoLSK} is the bit error probability of the DPolSK modulation which can be computed numerically using the double integration defined in [16, Eq. (42)]. The first term in (17) accounts for the random decision of the DPSK detector when errors occur in the DPolSK detector. In addition, $P_{\text{DPSK|DPoLSK}}$ is the conditional error probability of the DPSK given the correction of the DPolSK detector which is defined for binary DPSK as [17]

$$P_{\text{DPSK|DPoLSK}} = \frac{1}{2} e^{\frac{-2\gamma}{N_o}}, \tag{18}$$

while for higher DPSK modulation orders, an approximation assuming a 3dB reduction of the DPSK compared to coherent PSK can be used as [17]

$$P_{\text{DPSK|DPoLSK}} \approx \frac{2}{\log_2(K)} Q\left\{ \sqrt{\frac{\gamma}{N_o}} \left(\sin(\pi/K) \right) \right\}, \tag{19}$$

where $Q\{.\}$ denotes the Gaussian Q-function, while gray coding in symbol mapping is assumed. Moreover, the overall bit error ratio (BER) of the entire transmission, considering the different rates between the binary DPolSK and K-DPSK becomes

$$\text{BER} \approx \frac{P_{\text{DPoLSK}} + \log_2(K) P_{\text{DPSK}}}{1 + \log_2(K)}. \tag{20}$$

TABLE I: Simulation Parameters

Parameter	Value
Gain of antennas (G_t, G_r)	3 dBi
Carrier frequency	30 GHz
Noise power (N_o)	-96 dBm
Number of RIS elements (M)	17×17
Location of source	$[10, 0, 0]\, m$
Location of Receiver	$[10, 20, 0]\, m$
Location of RIS	$[0, 10, 0]\, m$
Frame length (T)	1000

VI. Simulation Results

In this section, we evaluate the performance of the proposed JDPPM scheme. The simulation parameters are as shown in Table I. In Fig. 3a, we compare the performance of the proposed JDPPM scheme with the joint coherent polarization and phase modulation (JCPPM) scheme, both employing QPSK modulation ($K = 4$). The JCPPM utilizes coherent modulations, requiring CSI estimation at the receiver. It is clear that the heuristic analytical performance of the JDPPM closely aligns with the simulated results. Despite the JDPPM exhibiting inferior performance compared to JCPPM, it offers the advantage of non-coherent detection, eliminating the need for CSI estimation. Conversely, the JCPPM is sensitive to CSI estimation errors, which for simplicity, are modeled in terms of the orientation angle estimation error in (2) as $\hat{\beta} = \beta + e_c$, where e_c is modeled as a zero-mean Gaussian distribution, $e_c \sim \mathcal{N}_{\mathcal{R}}(0, \sigma_c^2)$. Moreover, the JDPPM is sensitive to the channel variation between consecutive time slots, which is modeled between the ith and $(i-1)$th time slots as $\beta_i = \beta_{i-1} + e_d$, where $e_d \sim \mathcal{N}_{\mathcal{R}}(0, \sigma_d^2)$.

In Fig. 3b, we dissect the performance of the JDPPM to examine the influence of the two-stage detector, in terms of the error propagation. We simulate the performance for $K = 2, 4$, and 8. The performance of DPolSK detection and the DPSK detection conditioned by the correctness of DPolSK are depicted separately to analyze their individual contributions to the overall performance. It is clear that the performance of JDPPM is predominantly influenced by DPolSK detection for $K \leq 4$, whereas it becomes dominated by DPSK at higher modulation orders.

In Fig. 3c, we compare the performance of the proposed JDPPM with two benchmark schemes capable of non-coherent reception. The first scheme solely performs DPSK modulation [6]. The second scheme performs pulse amplitude modulation (PAM) by turning on/off the RIS elements to control the received signal strength[18]. To ensure a fair comparison, we maintain an equal number of bits per channel use. Thus, we compare the JDPPM with $K = 2, 4$, and 8 against DPSK and PAM with $K = 4, 8$, and 16, respectively. It is clear that JDPPM has better performance when $K \geq 4$.

This article has been accepted for publication in IEEE Wireless Communications Letters. This is the author's version which has not been fully edited and content may change prior to final publication. Citation information: DOI 10.1109/LWC.2024.3496257

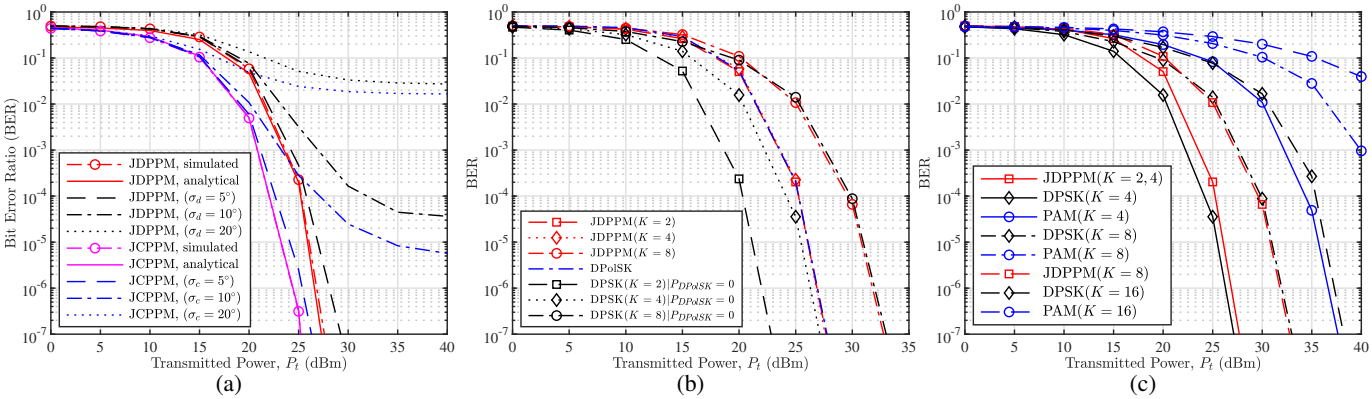

Fig. 3: In (a) JDPPM versus JCPPM, (b) JDPPM performance deconstructed into DPSK and DPolSK performances, and (c) RIS-assisted JDPPM versus RIS-assisted DPSK and RIS-assisted PAM.

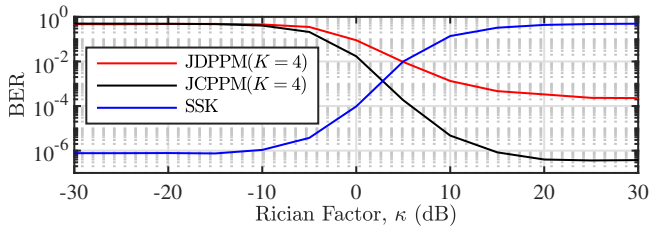

Fig. 4: Performance comparison between RIS-assisted JDPPM and RIS-assisted SSK versus the Rician fading factor.

In Fig. 4, we compare the JDPPM against another benchmark scheme [2] where a RIS comprising single-polarized elements performs space shift keying (SSK) modulation and utilizes a greedy detector which demodulates based on the received antenna index with the highest signal strength, enabling non-coherent reception. We model the channel as a Rician fading channel and compare the performance versus the Rician fading factor denoted as κ, at $P_t = 25$ dBm, where, $\kappa = \infty$ represents a LoS channel, while $\kappa = 0$ indicates a Rayleigh fading channel. An important trade-off emerges between JPPM and SSK: as the channel exhibits less scattering, the received signals become more correlated in the spatial domain, leading to degraded performance of SSK. Conversely, in rich scattering channels, the SoPs of multipath components combine at the receiver, resulting in performance deterioration due to fluctuations in SoP controlled by the RIS.

VII. Conclusion

We developed a RIS-based information transfer scheme for non-coherent polarized receivers. The RIS is configured to jointly establish beamforming and develop a differential polarization modulation by manipulating the polarization states of the reflecting signals. Then, an additional DPSK modulation layer is overlaid either by the source or the RIS, subject to the source-to-RIS feedback channel existence. The proposed scheme enables non-coherent detection with immunity to CSI errors. Furthermore, it facilitates RIS-based information transfer schemes in highly correlated environments, contrasting with RIS-based spatial modulation schemes.

References

[1] E. Basar, "Transmission through large intelligent surfaces: A new frontier in wireless communications," in *2019 European Conference on Networks and Communications (EuCNC)*. IEEE, 2019, pp. 112–117.

[2] E. Basar, "Reconfigurable intelligent surface-based index modulation: A new beyond MIMO paradigm for 6g," *IEEE Transactions on Communications*, vol. 68, no. 5, pp. 3187–3196, 2020.

[3] E. Ibrahim, R. Nilsson, and J. Van De Beek, "Binary polarization shift keying with reconfigurable intelligent surfaces," *IEEE Wireless Communications Letters*, vol. 11, no. 5, pp. 908–912, 2022.

[4] S. Guo, S. Lv, H. Zhang, J. Ye, and P. Zhang, "Reflecting modulation," *IEEE Journal on Selected Areas in Communications*, vol. 38, no. 11, pp. 2548–2561, 2020.

[5] S. Guo, J. Ye, P. Zhang, H. Zhang, and M.-S. Alouini, "Differential reflecting modulation for reconfigurable intelligent surface-based communications," *IEEE Communications Letters*, vol. 25, no. 3, pp. 907–910, 2020.

[6] J. Ino, H. Wakatsuchi, and S. Sugiura, "Noncoherent reconfigurable intelligent surface with differential modulation and reflection pattern training," *IEEE Wireless Communications Letters*, 2023.

[7] S. W. Ellingson, "Path loss in reconfigurable intelligent surface-enabled channels," in *2021 IEEE 32nd Annual International Symposium on Personal, Indoor and Mobile Radio Communications (PIMRC)*. IEEE, 2021, pp. 829–835.

[8] X. Zhu, W. Chen, Z. Li, Q. Wu, Z. Zhang, K. Wang, and J. Li, "RIS-aided spatial scattering modulation for mmWave MIMO transmissions," *IEEE Transactions on Communications*, 2023.

[9] X. Zhu, L. Yuan, K. J. Kim, Q. Li, and J. Zhang, "Reconfigurable intelligent surface-assisted spatial scattering modulation," *IEEE Communications Letters*, vol. 26, no. 1, pp. 192–196, 2021.

[10] Y. Han, X. Li, W. Tang, S. Jin, Q. Cheng, and T. J. Cui, "Dual-polarized RIS-assisted mobile communications," *IEEE transactions on wireless communications*, vol. 21, no. 1, pp. 591–606, 2021.

[11] M. Coldrey, "Modeling and capacity of polarized MIMO channels," in *VTC Spring 2008-IEEE Vehicular Technology Conference*. IEEE, 2008, pp. 440–444.

[12] L. Jiang, L. Thiele, and V. Jungnickel, "On the modelling of polarized MIMO channel," *Proc. Europ. Wireless*, vol. 2007, pp. 1–4, 2007.

[13] E. Björnson, J. Hoydis, and L. Sanguinetti, "Massive MIMO networks: Spectral, energy, and hardware efficiency," *Foundations and Trends in Signal Processing*, vol. 11, no. 3-4, pp. 154–655, 2017.

[14] C. You, B. Zheng, and R. Zhang, "Fast beam training for IRS-assisted multiuser communications," *IEEE Wireless Communications Letters*, vol. 9, no. 11, pp. 1845–1849, 2020.

[15] C. Guo, F. Liu, S. Chen, C. Feng, and Z. Zeng, "Advances on exploiting polarization in wireless communications: Channels, technologies, and applications," *IEEE Communications Surveys & Tutorials*, vol. 19, no. 1, pp. 125–166, 2016.

[16] S. Benedetto and P. Poggiolini, "Theory of polarization shift keying modulation," *IEEE Transactions on communications*, vol. 40, no. 4, pp. 708–721, 1992.

[17] M. K. Simon and M.-S. Alouini, *Digital communication over fading channels*. New York: Wiley, 2001.

[18] W. Yan, X. Yuan, and X. Kuai, "Passive beamforming and information transfer via large intelligent surface," *IEEE Wireless Communications Letters*, vol. 9, no. 4, pp. 533–537, 2019.